energies

MDPI

Article

Distributed Optimization of District Heating Networks Using Optimality Condition Decomposition

Jona Maurer *, Jochen Illerhaus, Pol Jané Soneira and Sören Hohmann

Institute of Control Systems (IRS), Karlsruhe Institute of Technology (KIT), Kaiserstraße 12, 76131 Karlsruhe, Germany

* Correspondence: jona.maurer@kit.edu

Abstract: The optimal operation of District Heating Networks (DHNs) is a challenging task. Current or future optimal dispatch energy management systems attempt to optimize objectives, such as monetary cost minimization, emission reduction, or social welfare maximization. Typically, this requires highly nonlinear models and has a substantial computational cost, especially for large DHNs. Consequently, it is difficult to solve the resulting nonlinear programming problem in real time. In particular, as typical applications allow for no more than several minutes of computation time. However, a distributed optimization approach may provide real time performance. Thereby, the solution of the central optimization problem is obtained by solving a set of small-scale, coupled optimization problems in parallel. At runtime, information is exchanged between the small-scale problems during the iterative solution procedure. A well-known approach of this class of distributed optimization algorithms is Optimality Condition Decomposition (OCD). Important advantages of this approach are the low amount of information exchange needed between the small-scale problems and that it does not require the tuning of parameters, which can be challenging. However, the DHNs model equation structure brings along many difficulties that hamper the application of the OCD approach. Simulation results demonstrate the applicability range of the presented method.

Keywords: district heating networks; optimal dispatch; nonlinear optimization; distributed optimization; optimality condition decomposition; electric power networks

check for updates

Citation: Maurer, J.; Illerhaus, J.; Soneira, P.J.; Hohmann, S. Distributed Optimization of District Heating Networks Using Optimality Condition Decomposition. *Energies* **2022**, *15*, 6605. https://doi.org/10.3390/en15186605

Academic Editors: Carlos Pozo and Ángel Galán Martín

Received: 11 August 2022
Accepted: 5 September 2022
Published: 9 September 2022

Publisher's Note: MDPI stays neutral with regard to jurisdictional claims in published maps and institutional affiliations.

Copyright: © 2022 by the authors. Licensee MDPI, Basel, Switzerland. This article is an open access article distributed under the terms and conditions of the Creative Commons Attribution (CC BY) license (https://creativecommons.org/licenses/by/4.0/).

1. Introduction

Optimal operation of District Heating Networks (DHNs) is a major task to lower emissions, operation costs, network losses or to maximize the social welfare in market-based forms of DHN operation. Thereby, the optimal DHN operation regarded within this work is understood as a form of dispatch for producers and flexible loads, which is performed after a previously applied unit commitment (unit commitment is not within the scope of this work); see, e.g., [1] for operation and control hierarchies in DHN operation. The operational optimization problem is formulated as a Nonlinear Programming (NLP) problem, and an overview on the kinds of operational optimization problems used for DHNs is given in [2].

The most efficient form of DHN operation comprises variables mass flows [3], Variable Mass Flow Directions (VMFDs) [4] and variable temperatures [5]. Thereby, the operation points of pumps, valves and the heat power injection and demand of all flexible network participants are set by an Energy Management System (EMS). Note that these flexible network participants can be producers, consumers, energy converters or thermal storage systems. When representing the physics of variable flows and variable temperatures in a mathematical model for operational optimization in an EMS, the computational burden becomes high for large real-world DHNs [6]. In certain cases, the resulting calculation times can surpass the desired time interval used for the operational optimization.

Simulations performed by the authors of this work, using a rolling horizon approach, where the operational NLP problem was implemented in GAMS and solved by the IPOPT

solver, for one of the 15 largest DHNs in Germany, showed calculation times above 15 min for prediction horizons larger than four time steps. Since prediction horizons in this range are low compared with the thermal transient propagation of temperature fronts throughout the DHN, the results of the optimizations can therefore most likely be increased for larger optimization horizons.

As time step intervals used in energy management systems for market and control frameworks for these kinds of systems are often within 15 min [7], further measures are needed to enable real time capability of the EMSs. The demand for further measures to reduce calculation times for future network operation becomes even more apparent in the light of an increasing number of flexible network participants needing to be coordinated in future DHNs [8]. These result from the necessity to decarbonize future heat supplies, and thus, increasingly, small producers, such as renewable energy sources, heat pumps, power-to-heat devices or waste heat suppliers (such as data centers, refrigerated warehouses and purification plants), are being connected to DHNs [8], replacing the earlier centralized power plants.

A well-known measure to reduce calculation times is the parallelization of computations by decomposing the original central operational optimization problem into multiple coupled small-scale subproblems, which are then solved in a coordinated manner. Different approaches for parallelization are presented in [9,10]. A large field of literature is provided for the distributed optimization of electric power networks or coupled electric power and district heating networks [11–19]. Most of the distributed optimal operation approaches use the Alternating Direction Method of Multipliers (ADMM) [20] or the Optimality Condition Decomposition (OCD) [21] algorithms.

All the stated approaches decompose the operational optimization problems for the energy systems into small-scale subproblems, by dividing the energy network models into multiple zones, which are then optimized in parallel by multiple EMSs. However, the mentioned approaches all decompose the energy networks within electric power networks or at the boundary of electric power and district heating networks. Thus far, almost no work exists that decomposes the DHNs themselves into subproblems. Important advantages of the OCD approach are the low amount of information exchange needed between the small-scale problems and that it does not require the tuning of parameters, which can be challenging [16]. These tuning procedures are needed for ADMM approaches [9]. Further, the OCD approach enables real parallelization, while ADMM uses sequential calculations in its standard form [20].

Note that these sequential calculations also include computations by a central coordinating instance for ADMM approaches. Thus, three sequential calculations need to be performed for every iteration of the ADMM algorithm [20]. Furthermore, a convergence criterion is provided in the literature for OCD [21], which enables to compare different forms of decomposition by convergence speed. This criterion can be used to compare different forms of network decomposition with each other [22].

Through the symmetrical flow conditions in DHNs in the supply and return networks, the coupling of the subproblems arising from a certain decomposition is inherently large in DHNs. This impedes the straight-forward application of the OCD approach, as strong couplings between the subproblems prevent fulfillment of the convergence condition. Thus, an adequate reformulation of the operational optimization model is needed, which represents the physical effects with similar precision but reduces the coupling of the subproblems.

To the best of the authors' knowledge, thus far, the field of distributed optimization of DHNs is barely researched. An approach for distributed optimization of DHNs based on the ADMM is presented in [23]. As far as we know, the literature does not provide any approaches applying OCD to DHNs. Thus, we would like to bridge that gap and provide a distributed optimization approach that can be solved in parallel. Therefore, the contributions of this paper are:

- A new approach for the distributed optimal operation of DHNs based on OCD.

- In order to enable the application of OCD, the inherently strong coupling of small scale subproblems needs to be reduced by an adequate model reformulation. Thereby, the relevant physical effects are further accurately described.

1.1. Notation

Column vectors $\boldsymbol{x} \in \mathbb{R}^n$ are represented with boldface lowercase letters, matrices $\boldsymbol{A} \in \mathbb{R}^{n \times n}$ with boldface capital letters. For simplicity, we represent a vector composed of two stacked column vectors as $\boldsymbol{x} = [\boldsymbol{x}_1, \boldsymbol{x}_2]$. The notation $\nabla_{\boldsymbol{x}} f$ is defined as the partial derivative of f w.r.t. $\boldsymbol{x}$. We denote $\boldsymbol{x}^\top$ as the transpose of vector $\boldsymbol{x}$.

1.2. Structure

The rest of this paper is organized as follows: Section 2 explains the basic principles and properties of the OCD algorithm. Further, Section 3 provides the operational optimization model of the DHN, the reformulation needed for OCD and the final OCD approach for DHN operation. A proof of principle is given based on the simulation results in Section 4. Finally, a discussion is found in Section 5.

2. Optimality Condition Decomposition

In this section, the OCD algorithm first presented in [21] is briefly reviewed. The decomposition approach of OCD is presented here without loss of generality for the case of two subproblems/operational zones, marked with the superscripts $^{\mathrm{za}}$ and $^{\mathrm{zb}}$ below. An exemplary central optimization problem used to illustrate the approach is given as [10]:

$$\min_{\boldsymbol{x}^{\mathrm{za}}, \boldsymbol{x}^{\mathrm{zb}}} \; f^{\mathrm{za}}\left(\boldsymbol{x}^{\mathrm{za}}\right) + f^{\mathrm{zb}}\left(\boldsymbol{x}^{\mathrm{zb}}\right) \tag{1a}$$

subject to

$$\boldsymbol{h}^{\mathrm{za}}\left(\boldsymbol{x}^{\mathrm{za}}, \boldsymbol{x}^{\mathrm{zb}}\right) = \boldsymbol{0}, \tag{1b}$$

$$\boldsymbol{h}^{\mathrm{zb}}\left(\boldsymbol{x}^{\mathrm{za}}, \boldsymbol{x}^{\mathrm{zb}}\right) = \boldsymbol{0} \tag{1c}$$

with the equality constraints divided into two parts, $\boldsymbol{h}^{\mathrm{za}}$ and $\boldsymbol{h}^{\mathrm{za}}$. We assume the global objective function is the sum of the objective functions of the operational zones, as these represent cost, and we aim to minimize the sum of all costs. Note that the optimization problem cannot be solved separately by the two operational zones, since the optimization problems are coupled through the coupling constraints (1b) and (1c) (also called complicating constraints). For reasons of simplicity, we neglect constraints that depend on one group of variables only, since they can be readily included [10,21]. Then, the Lagrangian of (1) is defined as:

$$\begin{aligned}\mathcal{L}\left(\boldsymbol{x}^{\mathrm{za}}, \boldsymbol{x}^{\mathrm{zb}}, \boldsymbol{\lambda}^{\mathrm{za}}, \boldsymbol{\lambda}^{\mathrm{zb}}\right) =& f^{\mathrm{za}}\left(\boldsymbol{x}^{\mathrm{za}}\right) + f^{\mathrm{zb}}\left(\boldsymbol{x}^{\mathrm{zb}}\right) \\ &+ \left(\boldsymbol{\lambda}^{\mathrm{za}}\right)^\top \boldsymbol{h}^{\mathrm{za}}\left(\boldsymbol{x}^{\mathrm{za}}, \boldsymbol{x}^{\mathrm{zb}}\right) + \left(\boldsymbol{\lambda}^{\mathrm{zb}}\right)^\top \boldsymbol{h}^{\mathrm{zb}}\left(\boldsymbol{x}^{\mathrm{za}}, \boldsymbol{x}^{\mathrm{zb}}\right).\end{aligned} \tag{2}$$

Setting up the Karush–Kuhn–Tucker (KKT) conditions and applying the Newton–Raphson method leads to the following set of equations that is solved for every Newton iteration ν [16]:

$$\underbrace{\begin{bmatrix} \mathbf{KKT}^{\mathrm{za}} & \mathbf{KKT}^{\mathrm{zb,za}} \\ \mathbf{KKT}^{\mathrm{za,zb}} & \mathbf{KKT}^{\mathrm{zb}} \end{bmatrix}}_{\mathbf{KKT}} \underbrace{\begin{bmatrix} \boldsymbol{\Delta}^{\mathrm{cent,za}} \\ \boldsymbol{\Delta}^{\mathrm{cent,zb}} \end{bmatrix}}_{\boldsymbol{\Delta}^{\mathrm{cent}}} = - \underbrace{\begin{bmatrix} \nabla_{[\boldsymbol{x}^{\mathrm{za}}, \boldsymbol{\lambda}^{\mathrm{za}}]} \mathcal{L} \\ \nabla_{[\boldsymbol{x}^{\mathrm{zb}}, \boldsymbol{\lambda}^{\mathrm{zb}}]} \mathcal{L} \end{bmatrix}}_{\nabla \mathcal{L}}, \tag{3}$$

with the Nabla operator ∇ and the search directions of the central problem given by $\boldsymbol{\Delta}^{\mathrm{cent,za}} = \left[\Delta \boldsymbol{x}^{\mathrm{cent,za}}, \Delta \boldsymbol{\lambda}^{\mathrm{cent,za}}\right]$ and $\boldsymbol{\Delta}^{\mathrm{cent,zb}} = \left[\Delta \boldsymbol{x}^{\mathrm{cent,zb}}, \Delta \boldsymbol{\lambda}^{\mathrm{cent,zb}}\right]$. Further, the KKT matrices are defined as [10]:

$$\mathbf{KKT}^{\mathrm{za}} = \begin{bmatrix} \nabla^2_{\boldsymbol{x}^{\mathrm{za}},\boldsymbol{x}^{\mathrm{za}}}\mathcal{L} & \left(\nabla_{\boldsymbol{x}^{\mathrm{za}}}\boldsymbol{h}^{\mathrm{za}}\right)^\top \\ \nabla_{\boldsymbol{x}^{\mathrm{za}}}\boldsymbol{h}^{\mathrm{za}} & \mathbf{0} \end{bmatrix}, \quad \mathbf{KKT}^{\mathrm{zb,za}} = \begin{bmatrix} \nabla^2_{\boldsymbol{x}^{\mathrm{zb}},\boldsymbol{x}^{\mathrm{za}}}\mathcal{L} & \left(\nabla_{\boldsymbol{x}^{\mathrm{za}}}\boldsymbol{h}^{\mathrm{zb}}\right)^\top \\ \nabla_{\boldsymbol{x}^{\mathrm{zb}}}\boldsymbol{h}^{\mathrm{za}} & \mathbf{0} \end{bmatrix},$$
$$\mathbf{KKT}^{\mathrm{za,zb}} = \left(\mathbf{KKT}^{\mathrm{zb,za}}\right)^\top, \quad \mathbf{KKT}^{\mathrm{zb}} = \begin{bmatrix} \nabla^2_{\boldsymbol{x}^{\mathrm{zb}},\boldsymbol{x}^{\mathrm{zb}}}\mathcal{L} & \left(\nabla_{\boldsymbol{x}^{\mathrm{zb}}}\boldsymbol{h}^{\mathrm{zb}}\right)^\top \\ \nabla_{\boldsymbol{x}^{\mathrm{zb}}}\boldsymbol{h}^{\mathrm{zb}} & \mathbf{0} \end{bmatrix}. \tag{4}$$

The OCD approach decomposes the optimization problem (1) in a special manner into the following two subproblems, for Zone a:

$$\min_{\boldsymbol{x}^{\mathrm{za}}} \; f^{\mathrm{za}}\left(\boldsymbol{x}^{\mathrm{za}}\right) + \left(\overline{\boldsymbol{\lambda}}^{\mathrm{zb}}\right)^\top \boldsymbol{h}^{\mathrm{hb}}\left(\boldsymbol{x}^{\mathrm{za}}, \overline{\boldsymbol{x}}^{\mathrm{zb}}\right) \tag{5a}$$

subject to

$$\boldsymbol{h}^{\mathrm{za}}\left(\boldsymbol{x}^{\mathrm{za}}, \overline{\boldsymbol{x}}^{\mathrm{zb}}\right) = \mathbf{0}, \tag{5b}$$

and Zone b:

$$\min_{\boldsymbol{x}^{\mathrm{zb}}} \; f^{\mathrm{zb}}\left(\boldsymbol{x}^{\mathrm{zb}}\right) + \left(\overline{\boldsymbol{\lambda}}^{\mathrm{za}}\right)^\top \boldsymbol{h}^{\mathrm{za}}\left(\overline{\boldsymbol{x}}^{\mathrm{za}}, \boldsymbol{x}^{\mathrm{zb}}\right) \tag{6a}$$

subject to

$$\boldsymbol{h}^{\mathrm{zb}}\left(\overline{\boldsymbol{x}}^{\mathrm{za}}, \boldsymbol{x}^{\mathrm{zb}}\right) = \mathbf{0} \tag{6b}$$

where the $\overline{\square}$ operator indicates that these (dual) variables are constant and considered as parameters in the respective subproblem. The complicating constraint of the other operational zone is included in the objective function of the regarded operational zone. All variables and constraints have been assigned to a certain operational zone, while, for the objective function, each operational zone only considers its own objective function. Further, (5b) and (6b) represent complicating constraints.

Complicating constraints are not only considered within their proper operational zone by the approach but also as soft constraints within the objectives of the other operational zones related through the complicating constraint, see (5) and (6). In either case, the respective $\overline{\square}$ parameters are obtained from the (dual) variables of the other operational zone from the last Newton iteration $v-1$. This indicates the basic OCD algorithm for every Newton iteration v:

1. Perform one Newton iteration of the two subproblems (5) and (6).
2. Exchange the parameters between the subproblems/operational zones, here $\overline{\boldsymbol{x}}^{\mathrm{za}}$, $\overline{\boldsymbol{x}}^{\mathrm{zb}}$, $\overline{\boldsymbol{\lambda}}^{\mathrm{za}}$ and $\overline{\boldsymbol{\lambda}}^{\mathrm{zb}}$.
3. Check if the stopping criterion is fulfilled. If it is not met yet, then calculate the next Newton iteration $v+1$ in step 1.

Different stopping criteria are stated in the given literature [16,21]. Computing these distributed subproblems with Newton's method is equal to solving the following set of equations within every Newton iteration [16]:

$$\underbrace{\begin{bmatrix} \mathbf{KKT}^{\mathrm{za}} & \mathbf{0} \\ \mathbf{0} & \mathbf{KKT}^{\mathrm{zb}} \end{bmatrix}}_{\overline{\mathbf{KKT}}} \underbrace{\begin{bmatrix} \boldsymbol{\Delta}^{\mathrm{dist,za}} \\ \boldsymbol{\Delta}^{\mathrm{dist,zb}} \end{bmatrix}}_{\boldsymbol{\Delta}^{\mathrm{dist}}} = -\begin{bmatrix} \nabla_{[\boldsymbol{x}^{\mathrm{za}},\boldsymbol{\lambda}^{\mathrm{za}}]}\mathcal{L} \\ \nabla_{[\boldsymbol{x}^{\mathrm{zb}},\boldsymbol{\lambda}^{\mathrm{zb}}]}\mathcal{L} \end{bmatrix}, \tag{7}$$

with the distributed search directions $\boldsymbol{\Delta}^{\mathrm{dist,za}} = \left[\Delta\boldsymbol{x}^{\mathrm{dist,za}}, \Delta\boldsymbol{\lambda}^{\mathrm{dist,za}}\right]$ and $\boldsymbol{\Delta}^{\mathrm{dist,zb}} = \left[\Delta\boldsymbol{x}^{\mathrm{dist,zb}}, \Delta\boldsymbol{\lambda}^{\mathrm{dist,zb}}\right]$ as well as the approximated KKT matrix $\overline{\mathbf{KKT}}$. By comparing (7) with (3), it is understood that $\overline{\mathbf{KKT}}$ is obtained from $\mathbf{KKT}$ by setting the matrices on the secondary diagonals to $\mathbf{0}$. Now, convergence of the distributed solution towards the central solution of (1) can be shown if, at the provided second-order KKT point $\boldsymbol{y}^* = \left[\boldsymbol{x}^{\mathrm{za}}, \boldsymbol{x}^{\mathrm{zb}}, \boldsymbol{\lambda}^{\mathrm{za}}, \boldsymbol{\lambda}^{\mathrm{zb}}\right]$, the following holds [21]:

Assumption 1. *The second-order derivatives of* f^{za}, f^{zb}, $\boldsymbol{h}^{\mathrm{za}}$ *and* $\boldsymbol{h}^{\mathrm{zb}}$ *are Lipschitz continuous.*

Assumption 2. *The Jacobian matrix of the equality constraints of* (1)*, precisely* $\left[(\nabla \boldsymbol{h}^{\mathrm{za}})^{\top}, (\nabla \boldsymbol{h}^{\mathrm{zb}})^{\top}\right]^{\top}$ *provides full row rank.*

Note that Assumption 2 is fulfilled if the gradients of the constraints are linearly independent. This is not fulfilled if the system has, e.g., identical, parallel lines between two nodes. Last but not least, the condition for convergence given below needs to hold at $\boldsymbol{y}^*$ [21]:

Condition 1.

$$\rho^{\mathrm{ocd},*} = \rho\left(\boldsymbol{I} - \left(\overline{\mathbf{KKT}}^*\right)^{-1}\mathbf{KKT}^*\right) < 1, \tag{8}$$

with $\rho(\square)$ defining the spectral radius, which equals the absolute value of the maximal eigenvalue of the given matrix. Further, $\mathbf{KKT}^*$ represents the KKT matrix at the optimal solution. If Assumptions 1 and 2 are fulfilled, and Condition 1 is fulfilled as well, then iteratively solving (5) and (6) will converge towards $\boldsymbol{y}^*$ with at least linear rate $\rho^{\mathrm{ocd},*}$ for all starting points $\boldsymbol{y}^0$ sufficiently close to $\boldsymbol{y}^*$. The literature often refers to $\rho^{\mathrm{ocd},*}$ as the coupling factor. As can be understood from Equation (8), the coupling factor is smaller for decompositions possessing less coupling, since then less non zero entries on the secondary diagonals of the KKT block matrix $\mathbf{KKT}^{\mathrm{za,zb}}$ and $\mathbf{KKT}^{\mathrm{zb,za}}$ are neglected in $\overline{\mathbf{KKT}}^*$. In the context of optimal dispatch of energy systems, this refers to less tie lines or pipelines connecting the decoupled operational zones [16].

Within the following remarks further important aspects of the OCD approach w.r.t. the present work are described.

Remark 1. *The OCD approach, which was presented here for the simple case of an optimization problem with complicating constraints, can be simply expanded to the case of additional non complicating equality and inequality constraints, which only include variables of the respective operational zone. Furthermore, complicating inequality constraints, such as flow limits over border edges, can be readily included in the same manner as complicating equality constraints [24].*

Remark 2. *There are indications that symmetrically decomposed problems are more likely to fulfill Condition 1. Symmetrical decomposition means that a complicating constraint in both operational zones is present, which has an identical part and incorporates the same (parameterized) variables. The first indication is that the majority of the published applications of OCD to energy system dispatch problems decompose the central problems in a symmetrical form. For example, in optimal power flow problems, the power flow over a tie line* $P_{i,j}^{\mathrm{flow}}$ *is part of the power flow constraints, of both border nodes in the two adjacent operational zones and given by:*

$$P_{i,j}^{\mathrm{flow}} = V_i V_j [B_{i,j}^{\mathrm{bus}} \sin(\theta_i - \theta_j) + G_{i,j}^{\mathrm{bus}} \cos(\theta_i - \theta_j)] \tag{9}$$

This power flow is dependent on the voltage angle θ *and voltage amplitude* V *of the bordering nodes* i *and* j*, which are thus part of both complicating constraints [16,25]. The parameters* B^{bus} *and* G^{bus} *represent the susceptance and conductance of the nodal admittance matrix used to model the electric power network for alternating current power flow calculations. Furthermore, it becomes clear by comparing the structure of the* $\overline{\mathbf{KKT}}$ *and* $\mathbf{KKT}$ *matrices that the distributed search directions* $\boldsymbol{\Delta}^{\mathrm{dist}}$ *in* (7) *will most likely be closer to the central search direction* $\boldsymbol{\Delta}^{\mathrm{cent}}$ *in* (3) *if all operational zones take information of the other (bordering) operational zones into account, while calculating* $\boldsymbol{\Delta}^{\mathrm{dist}}$*.*

Remark 3. *The decomposition of a central optimization problem into many coupled but smaller subproblems achieves a considerable reduction of the computation time. In [21], it is shown that even solving the small scale subproblems sequentially on only one processor, the computation time is less than computing the solution of the central problem directly. Note that this computation time*

can be lowered by orders of magnitude by further parallelizing the subproblems and solving them in a coordinated manner. This is due to the bad scaling of the computation time with the number of optimization variables in nonlinear programming; it is more efficient to solve many small scale problems sequentially.

3. Optimal Dispatch of District Heating Networks Using Optimality Condition Decomposition

This section first introduces the central optimization problem used in this work to optimize DHN operation. Based on this, the model reformulation needed to reduce the coupling of the subproblems when applying OCD is presented next. Finally, the application of OCD to the resulting problem is provided including the complicating constraints and the resulting objective functions arising from the OCD approach for each zone are provided.

3.1. Central Optimization Problem for Optimal Dispatch of District Heating Networks

The nonlinear programming problem used for operational optimization of DHNs used within this paper is given in the following. This comprises the objective function, the equality constraints, as well as box constraints limiting the permissible range of all variables.

3.1.1. Objective Function

The objective function f, which can, in general, represent emissions, operation costs, network losses or renewable energy sources curtailment, which should by minimized. A further possibility that is used in this work is to maximize the social welfare in a market-based form of DHN operation, such as those provided in [26].

3.1.2. Equality Constraints

This section briefly describes the DHN models used within this work. In particular, the hydraulic and thermal models of nodes, pipelines, consumers and producers are provided. The DHN network graph is spanned by the node edge incidence matrix, defined as (cf. [27])

$$A_{i,e} = \begin{cases} 1, \text{ if } e \text{ is directed towards } i \\ -1, \text{ if } e \text{ is directed away from } i \\ 0, \text{ if } e \text{ is not connected to } i. \end{cases} \qquad \forall\, i \in \mathbb{S}_i, e \in \mathbb{S}_e \tag{10}$$

where i represents a node from the set of all network nodes $\mathbb{S}_i$, and e is a respective edge from all edges $\mathbb{S}_e$.

Hydraulic Model

The models of all typical hydraulic elements are given below. For all components representing DHN edges e, a general stationary relation of the mass flow $\dot{m}$ and the pressure difference Δp can be defined for all regarded time steps $k \in \mathbb{S}_k$ as:

$$\Delta p_{e,k} = -\sum_{i \in \mathbb{S}_i} A_{i,e} p_{i,k} = \beta_{e,k} + \mu_{e,k} \dot{m}_{e,k} |\dot{m}_{e,k}|_{\Delta\varepsilon} \qquad \forall\, e \in \mathbb{S}_e,\ k \in \mathbb{S}_k \tag{11}$$

where β and μ are the variable component coefficients and p_i represents the nodal pressure at node i. For pipelines, the values of β and μ are calculated as given in [4], and the Prandtl–Colebrook equation is simplified using the Haaland approximation [28]. Thereby, turbulent flow conditions are assumed [4]. For consumers, we assume $\beta = 0$ and μ is to be within the box constraints, which are defined by the parameters of the valve and the heat exchanger within the consumer. Further, producers are assumed to contain a pump, a heat exchanger and a valve. The pumps can vary the value of the box constrained β, while the rest of the producers are modeled as consumers, thus, with a constrained value μ. Note that (11) is continuously differentiable as the absolute value function of the mass flow $\dot{m}$ is replaced by a continuous differentiable approximation given by:

$$|\dot{m}_{e,k}|_{\Delta\varepsilon} = \sqrt{\Delta\varepsilon + (\dot{m}_{e,k})^2} \tag{12}$$

wherein $\Delta\varepsilon > 0$ is a sufficiently small parameter. In case of a predefined positive flow direction (positive flow direction equals the edge orientation), when the e is not element of the set of all edges with VMFDs, $\mathbb{S}_e^{\text{vmfd}}$, (11) can be written as

$$-\sum_{i\in\mathbb{S}_i^{ht}} A_{i,e}p_{i,k} = \beta_{e,k} + \mu_{e,k}(\dot{m}_{e,k})^2 \qquad \forall\, e \in \mathbb{S}_e, e \notin \mathbb{S}_e^{\text{vmfd}},\ k \in \mathbb{S}_k \tag{13}$$

The law of conservation of mass is represented by (14) for all mass flows entering and leaving a node i:

$$\sum_{e\in\mathbb{S}_e} A_{i,e}\dot{m}_{e,k} = 0 \qquad \forall\, i \in \mathbb{S}_i,\ k \in \mathbb{S}_k \tag{14}$$

Thermal Model

For all nodes $\mathbb{S}_i^{\text{vmfd}} \subset \mathbb{S}_i$ where, at least on one connected edge, a flow direction change can take place, the node temperature T_i is calculated by the heat balance equation, considering all possible flow conditions as given in [4]:

$$\begin{aligned} & T_{i,k} \sum_{e\in\mathbb{S}_e} \left(A_{i,e}^{-} \max\left(\dot{m}_{e,k}, 0\right) + A_{i,e}^{+} \max\left(-\dot{m}_{e,k}, 0\right)\right) \\ = & \sum_{e\in\mathbb{S}_e} \left(A_{i,e}^{+} \max(\dot{m}_{e,k}, 0) T_{e,k}^{\text{out}} + A_{i,e}^{-} \max(-\dot{m}_{e,k}, 0) T_{e,k}^{\text{in}}\right) \qquad \forall\, i \in \mathbb{S}_i^{\text{vmfd}}, k \in \mathbb{S}_k \end{aligned} \tag{15}$$

The right-hand side of Equation (15) contains the sum of all temperatures entering this node and leaving the respective edge T_e^{out}, or T_e^{in} in the case of negative flow, weighted by their mass flows $\dot{m}$. This has to equal the node temperature T_i, which is multiplied by the mass flows leaving the node. All possible cases, based on the varying mass flow directions in the pipelines, are distinguished by combining the incoming and leaving node edge incidence matrix elements $A_{i,e}^{+}$ and $A_{i,e}^{-}$ and the approximated maximum operator. The approximation is analogous to the absolute value function approximation in (12) and is defined as:

$$\max(\dot{m}_{e,k}, 0) \approx \frac{|\dot{m}_{e,k}|_{\Delta\varepsilon} + \dot{m}_{e,k}}{2} = \frac{\sqrt{\Delta\varepsilon + \dot{m}_{e,k}^2} + \dot{m}_{e,k}}{2} \tag{16}$$

The elements of the incoming and leaving edge node incidence matrices $\boldsymbol{A}^{+}$ and $\boldsymbol{A}^{-}$ of the DHN are defined as:

$$\begin{aligned} A_{i,e}^{+} &= \begin{cases} 1, & \text{if } A_{i,e} = +1 \\ 0, & \text{otherwise} \end{cases} \qquad \forall\, i \in \mathbb{S}_i, e \in \mathbb{S}_e \\ A_{i,e}^{-} &= \begin{cases} 1, & \text{if } A_{i,e} = -1 \\ 0, & \text{otherwise} \end{cases} \qquad \forall\, i \in \mathbb{S}_i, e \in \mathbb{S}_e \end{aligned} \tag{17}$$

For nodes without edges with VMFDs entering the node, the model Equation (15) is simplified to the form, e.g., found in [29].

Consumer and Producer

The heat power supply or demand Φ of producers and consumers is defined by the following equation throughout the existing literature, such as those given in [30]:

$$\Phi_{e,k} = c^{\text{w}} \dot{m}_{e,k} (T_{e,k}^{\text{out}} - T_{e,k}^{\text{in}}) \qquad \forall\, e \in \mathbb{S}_e^{\text{exch}}, k \in \mathbb{S}_k \tag{18}$$

Pipelines are modeled as in [31] (Node Method Version 1b); thereby, we neglect the steal core model, as future DHN will not possess steal cores due to lower temperature operation values [8], and we precalculate the values y, z (in [31], y and z are written as n and m, which are already in use for other symbols in this paper), R and S before every optimization based on the mass flow values from the last optimization.

This precalculation of the respective parameters enables reducing the obtained mixed integer nonlinear programming to a nonlinear programming problem [32]. Further, the length of stay is calculated based on the formula presented in [32] and a predefined flow direction is assumed for model simplicity reasons. Note that pipelines crossing zone borders will be differently modeled in Section 3.3.

3.2. Model Reformulation for OCD

In the following, the necessity of the reformulation of the model presented in Section 3.1.2 is provided. Before starting, the following definition is provided. For the spatial form of decomposition applied in this work, all network elements will be assigned to a specific operational zone. Thereby, the following special network elements are defined:

Definition 1.

- ***Border edge**: An edge e crossing the border of two neighboring operational zones, e.g., Zone a and Zone b. Thereby, this border edge will be defined as a border edge in both neighboring operational zones a and b.*
- ***Border node**: A node i connected to a border edge e.*
- ***Border loop**: Border loops are loops l that have edges e in multiple operational zones.*

Condition 1 is easily violated when OCD is applied to DHNs. This comes from the fact that decomposing DHN optimization model constraints as provided in Section 3.1.2 into subproblems directly results in multiple complicating constraints in every zone. This becomes clear with regard to the small example DHN presented in Figure 1. A naive decomposition into two operational areas Zone a and Zone b applied in this example, yields four complicating constraints for every zone in every time step.

This is due to the complicating constraints arising from (14) and (15) for both nodes in every zone. Based on the model presented in Section 3.1.2, the pipeline model equations would also bring along a complicating constraint. However, this can be prevented by using the Assumption 4, which enables replacing the thermal pipeline model by an identity function mapping the input temperature to the output temperature.

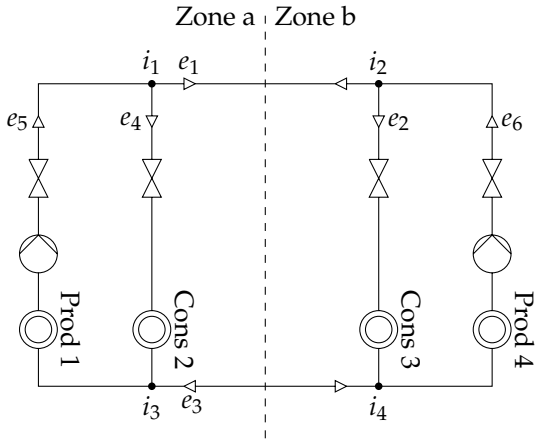

Figure 1. Example: *four-node network.* DHN with four nodes decomposed into Zones a and b.

From this example, it can be understood that the inherent strong coupling of DHNs results from the topology of DHNs, including the supply and a return network. In general, a stronger coupling of the subproblems, which is increased by every complicating constraint,

leads to higher values of $\rho^{\mathrm{ocd},*}$; see the paragraph on OCD in Section 2. Thus, the more complicating constraints exist, the more likely it is that Condition 1 is not met.

In contrast to DHNs, applying OCD to electric power networks only leads to a single complicating constraint in every zone for every border node [16], which is why OCD has been applied successfully for distributed optimization of electric power systems. From now on, we will restrict ourselves to the case of two zones, to reduce the notational burden and facilitate understanding of the provided methodology.

To reduce the coupling of the given problem, the hydraulic node Equation (14) of the border nodes in the return network, i_3 and i_4 in Figure 1 are omitted. Thereby, two complicating constraints of the form (21)—introduced and explained later on—are eliminated. However, by neglecting the hydraulic border nodes of the return networks, the model becomes incomplete, as the relation between mass flows and differential pressure of supply and return network on the border edges is not incorporated in the model anymore.

This gap is bridged by explicitly introducing the equality $\Delta p_1 = \Delta p_3$ for Figure 1, which can be notated as $p_1 - p_2 = p_4 - p_3$ or sorted by zones as $p_1 + p_3 = p_4 + p_2$ into the model. This also implies $\dot{m}_1 = \dot{m}_3$, based on (11). Using the loop edge incidence matrix B [27], this can be notated as:

$$\sum_{\substack{e \in \mathbb{S}_e^{\mathrm{za}} \\ e \notin \mathbb{S}_e^{\mathrm{be,za}}}} \sum_{i \in \mathbb{S}_i^{\mathrm{bi,za}}} |B_{l,e}||A_{i,e}| p_{i,k} = \sum_{\substack{e \in \mathbb{S}_e^{\mathrm{zb}} \\ e \notin \mathbb{S}_e^{\mathrm{be,zb}}}} \sum_{i \in \mathbb{S}_i^{\mathrm{bi,zb}}} |B_{l,e}||A_{i,e}| p_{i,k} \qquad \forall\, l \in \mathbb{S}_l^{\mathrm{bl}}, k \in \mathbb{S}_k \tag{19}$$

where the border loops are given in $\mathbb{S}_l^{\mathrm{bl}}$, and the border edges of Zone a $\mathbb{S}_e^{\mathrm{be,za}}$ represent a subset of the edges of Zone a given in $\mathbb{S}_e^{\mathrm{za}}$. The same notation is used for edges of Zone b, equivalently. If more then four nodes are found in the regarded border loop l, the relevant border nodes are found through $|B_{l,e}||A_{i,e}| = 1$ by checking this condition for all border nodes $i \in \mathbb{S}_i^{\mathrm{bi}}$ and edges e, which are no border edges (all border edges are given in $e \in \mathbb{S}_e^{\mathrm{be}}$) $e \in \mathbb{S}_e, e \notin \mathbb{S}_e^{\mathrm{be}}$ of the respective zone. For example, the left side of (19) can be simplified to $\sum_{i \in \mathbb{S}_i^{\mathrm{bi,za}}} p_{i,k}$ if only one point of coupling/border edge (in the return and supply network) to another zone exists as in Figure 1.

A further key aspect represents the artificial extension of the optimization problem used to enable a symmetrical form of decomposition in the following. Applying OCD to a central optimization problem with (19) as a complicating constraint would lead to an unsymmetrical decomposition, as this single equation is assigned either to Zone a or Zone b. Furthermore, representing the exact same Equation (19) twice in the central problem would lead to an undesired rank deficiency of the KKT matrix as explained in Assumption 2. This can be overcome by replacing (19) through the following two equations:

$$\begin{aligned} \sum_{e \in \mathbb{S}_e^{\mathrm{za}}, e \notin \mathbb{S}_e^{\mathrm{be,za}}} \sum_{i \in \mathbb{S}_i^{\mathrm{bi,za}}} |B_{l,e}||A_{i,e}| p_{i,k} &= p^{\mathrm{pre}} \\ \sum_{e \in \mathbb{S}_e^{\mathrm{zb}}, e \notin \mathbb{S}_e^{\mathrm{be,zb}}} \sum_{i \in \mathbb{S}_i^{\mathrm{bi,zb}}} |B_{l,e}||A_{i,e}| p_{i,k} &= p^{\mathrm{pre}} \end{aligned} \qquad \forall\, l \in \mathbb{S}_l^{\mathrm{bl}}, k \in \mathbb{S}_k \tag{20}$$

A comparison of these Equations (20) with the initial form (19) shows that the pressure potentials p_i of the nodes in the bordering zone have been replaced by the constant predefined pressure value p^{pre}. As p^{pre} is equal in both equations of (20), every solution fulfilling (20) will also satisfy Equation (19), since (20) is a special case of (19). The benefits of this new formulation are that the two equations in (20) are naturally assigned to their respective zones without creating further complicating constraints and thus reducing the coupling of the subproblems once more. Additionally, this procedure yields symmetrically decomposed subproblems. Further, the directions of the border edges are slightly varied as explained in the following remark.

Remark 4. *The decomposition only becomes fully symmetrical in the resulting border node Equations (21), (26), (29) and (31) outlaid below, by changing the edge directions of the border edges. As shown in Figure 1, edge e_1 is directed away from node i_1 and i_2, leading to $A_{i_1,e_1} = -1$ and $A_{i_2,e_1} = -1$. Analogously, e_3 is directed towards i_3 and i_4. Visually speaking, every zone calculates its solution with its own border edge directions, where the supply network border edge is directed away from the border node of the respective zone and the return network edge is directed to the proper border node of this zone. This is a deviation from the standard notation of the directed graph spanning up the DHN, where every edge is directed away from the start node and towards the end node. Still, the resulting system of equations is equivalent, as the differential pressure over the border edges Δp_e is defined using absolute values of $A_{i,e}$; see (23).*

3.3. Distributed Optimal Dispatch of DHNs Based on OCD

The following shows how optimal operation problems for DHNs can be solved in parallel by applying the OCD approach to the reformulated central optimization problem provided above within this Section 3.

The presented approach is based on the following assumptions, used for simplicity reasons:

Assumption 3. *Pipelines with VMFDs are the only component types for which edges can become border edges. These pipelines are not part of a mesh in the return or supply network. Furthermore, no control paths reach across zone borders.*

This is a valid assumption, as pipelines are the most common components in DHNs; thus, the limitations in finding possible decompositions for this assumption are manageable. Furthermore, as discussed after the upcoming assumption, the edges over which the approach decomposes the DHN can also be virtual pipelines.

Assumption 4. *The pipelines representing the border edges are regarded as negligibly short, and thus transmission delay, temperature losses and pressure potential differences due to height differences Δh (leading to $\beta > 0$ in the hydraulic pipeline model) are neglected here, as $\Delta h = 0$ is assumed.*

If this assumption would lead to unwanted deviations, due to a non negligible length of the pipeline, two artificial nodes and pipelines, one in the return and one in the supply network, could be introduced into the model in one of the zones at the end of the current border edge. Thereby, all parameters of the old border edge pipelines are kept the same, and the newly inserted pipelines, which are set as the new border edges, have the same parameters except for the pipeline length L, which is chosen as negligibly short.

For notational brevity, only the optimization problem of Zone a is fully stated, while the NLP of Zone b is directly evolvable thereof. All equations for every area, except the ones replaced by the complicating constraints and the new objectives stated here, stay the same as given in the previous subsections of Section 3.

The new hydraulic node equation, replacing (14) for supply network border nodes in Zone a, is given as (the extensive superscripts of h stand for: district heating network, hydraulic, supply network, border node and Zone a):

$$h_{i,k}^{\text{hydr,sn,bi,za}} = \sum_{\substack{e \in \mathbb{S}_e \\ e \notin \mathbb{S}_e^{\text{be}}}} A_{i,e} \dot{m}_{e,k} + \sum_{e \in \mathbb{S}_e^{\text{be}}} A_{i,e} \dot{m}_{e,k} = 0 \qquad \forall\, i \in \mathbb{S}_i^{\text{sn,bi,za}}, k \in \mathbb{S}_k \tag{21}$$

The main difference here to (14) is that border edges $e \in \mathbb{S}_e^{\text{be}}$ and "normal" edges $e \in \mathbb{S}_e, e \notin \mathbb{S}_e^{\text{be}}$ are distinguished. Border edge mass flows can then be expressed in dependence of pressure potentials p as stated below. Thereby, taking into account Assumption 4, which entails $\Delta h = 0$ and thus $\beta_{e,k} = 0$ in Equation (11):

$$\dot{m}_{e,k} \approx \operatorname{sgn}_{\Delta\varepsilon}(\Delta p_{e,k}) \sqrt{\frac{|\Delta p_{e,k}|_{\Delta\varepsilon}}{\mu_{e,k}(\dot{m}_{e,k})}} = \frac{1}{\sqrt{\mu_{e,k}(\dot{m}_{e,k})}} \frac{\Delta p_{e,k}}{\sqrt{|\Delta p_{e,k}|_{\Delta\varepsilon}}} \qquad \forall\, e \in \mathbb{S}_e^{\mathrm{be,za}}, k \in \mathbb{S}_k \tag{22}$$

The dependency of the pressure coefficient on the border edge mass flow $\mu_{e,k}(\dot{m}_{e,k})$ is eliminated by using a predefined pressure coefficient $\mu_{e,k}^{\mathrm{pre}}$. Alternatively, this pressure coefficient can be precalculated, based on the border edge mass flow of the previous optimization and (11), thus, using a similar procedure as effectively applied for the thermal pipeline model. Further, the differential pressure $\Delta p_{e,k}$ over the considered border edge e can be replaced by the difference of the pressure potential of the two connected border nodes i, from which one is in Zone a and the other in Zone b. Thus, the differential pressure over the border edge connected to a border node i of Zone a can be written as:

$$\Delta p_{e,k} = \sum_{i \in \mathbb{S}_i^{\mathrm{bi,za}}} \left(|A_{i,e}| p_{i,k} - \sum_{i' \neq i, i' \in \mathbb{S}_i} |A_{i',e}| \overline{p_{i',k}} \right) \qquad \forall\, e \in \mathbb{S}_e^{\mathrm{be,za}}, k \in \mathbb{S}_k. \tag{23}$$

By inserting (23) in (22) and exchanging the variable $\mu_{e,k}(\dot{m}_{e,k})$ by the parameter $\mu_{e,k}^{\mathrm{pre}}$, the mass flow on the border edge e itself is defined as:

$$\dot{m}_{e,k} \approx \frac{1}{\sqrt{\mu_{e,k}^{\mathrm{pre}}}} \frac{\sum\limits_{i \in \mathbb{S}_i^{\mathrm{bi,za}}} \left(|A_{i,e}| p_{i,k} - \sum\limits_{i' \neq i, i' \in \mathbb{S}_i} |A_{i',e}| \overline{p_{i',k}} \right)}{\sqrt{\left| \sum\limits_{i \in \mathbb{S}_i^{\mathrm{bi,za}}} \left(|A_{i,e}| p_{i,k} - \sum\limits_{i' \neq i, i' \in \mathbb{S}_i} |A_{i',e}| \overline{p_{i',k}} \right) \right|_{\Delta\varepsilon}}} \qquad \forall\, e \in \mathbb{S}_e^{\mathrm{be,za}}, k \in \mathbb{S}_k \tag{24}$$

For the network shown in Figure 1, Equation (23) is given by $\Delta p_{e_1,k} = p_{i_1,k} - p_{i_2,k}$ for Edge e_1 in Zone a. Based on this, the border edge mass flow $\dot{m}_{e_1,k}$ for Zone a stemming from Equation (24) results in:

$$\dot{m}_{e_1,k} \approx \frac{1}{\sqrt{\mu_{e_1,k}^{\mathrm{pre}}}} \frac{p_{i_1,k} - p_{i_2,k}}{\sqrt{|p_{i_1,k} - p_{i_2,k}|_{\Delta\varepsilon}}} \qquad \forall\, k \in \mathbb{S}_k \tag{25}$$

The thermal node equation, replacing (15) for border nodes, is formulated as follows (note that the border nodes are written separately to simplify the derivation of (31)):

$$\begin{aligned} h_{i,k}^{\mathrm{therm,bi,za}} = & T_{i,k} \Bigg[\sum_{\substack{e \in \mathbb{S}_e^{\mathrm{za}} \\ e \notin \mathbb{S}_e^{\mathrm{za,be}}}} \left(A_{i,e}^{-} \max\left(\dot{m}_{e,k}, 0\right) + A_{i,e}^{+} \max\left(-\dot{m}_{e,k}, 0\right) \right) + \\ & \sum_{e \in \mathbb{S}_e^{\mathrm{za,be}}} \left(A_{i,e}^{-} \max\left(\dot{m}_{e,k}, 0\right) + A_{i,e}^{+} \max\left(-\dot{m}_{e,k}, 0\right) \right) \Bigg] \\ & - \Bigg[\sum_{\substack{e \in \mathbb{S}_e^{\mathrm{za}} \\ e \notin \mathbb{S}_e^{\mathrm{za,be}}}} \left(A_{i,e}^{+} \max\left(\dot{m}_{e,k}, 0\right) T_{e,k}^{\mathrm{out}} + A_{i,e}^{-} \max\left(-\dot{m}_{e,k}, 0\right) T_{e,k}^{\mathrm{in}} \right) + \\ & \sum_{e \in \mathbb{S}_e^{\mathrm{za,be}}} \left(\left(A_{i,e}^{+} \max\left(\dot{m}_{e,k}, 0\right) + A_{i,e}^{-} \max\left(-\dot{m}_{e,k}, 0\right) \right) \sum_{\substack{i' \neq i \\ i' \in \mathbb{S}_i}} |A_{i,e}| |A_{i',e}| \overline{T_{i',k}} \right) \\ & \Bigg] = 0 \qquad \forall\, i \in \mathbb{S}_i^{\mathrm{bi,za}}, k \in \mathbb{S}_k \end{aligned} \tag{26}$$

Similarly to (21), the border mass flows are also defined by (24) in (26) above. With Assumption 4, supposing negligibly short pipelines between zones, the thermal pipeline model reduces to an identity function mapping the input temperature to the output temper-

ature here, $T_{i,k} = \overline{T}_{i',k}$ (however, more detailed models, such as a static pipeline model or a symmetric dynamic thermal pipeline model, could also be considered in the thermal node Equation (26)). For Node i_1 in Zone a in the DHN in Figure 1, Equation (26) is written as

$$\begin{aligned} & T_{i_1,k}\left[\max\left(\dot{m}_{e_1,k},0\right)+\max\left(\dot{m}_{e_4,k},0\right)+\max\left(-\dot{m}_{e_5,k},0\right)\right] \\ & -\left[\max\left(-\dot{m}_{e_4,k},0\right)T^{\text{in}}_{e_4,k}+\max\left(\dot{m}_{e_5,k},0\right)T^{\text{out}}_{e_5,k}+\max\left(-\dot{m}_{e_1,k},0\right)\overline{T_{i_2,k}}\right]=0 \\ & \forall\, k\in\mathbb{S}_k \end{aligned} \tag{27}$$

The resulting objective function for Zone a f^{za}, is defined as given below:

$$\begin{aligned} f^{\text{za}} = & f^{\text{rest,za}}+\sum_{k\in\mathbb{S}_k}\Bigg(\sum_{i\in\mathbb{S}_i^{\text{sn,bi,zb}}}\lambda_{i,k}^{\text{hydr,sn,bi,zb}}h_{i,k}^{\text{obj,hydr,sn,bi,zb}} \\ & +\sum_{i\in\mathbb{S}_i^{\text{bi,zb}}}\lambda_{i,k}^{\text{therm,bi,zb}}h_{i,k}^{\text{obj,therm,bi,zb}}\Bigg) \end{aligned} \tag{28}$$

This objective function f^{za} is composed of two parts. The first describes the decomposed objective of a central EMS $f(\boldsymbol{x})$. This comprises the objective $f'(\boldsymbol{x})$ resulting from a modification term $\delta \cdot \mathbf{I}$ with a small parameter δ and the identity matrix $\mathbf{I}$ added to the Hessian of the Lagrangian of the centralized and the distributed optimization problems to enhance convergence properties [33] (p. 574). The objective resulting from this modification is defined here as $f^{\text{rest,za}}$ for Zone a. The second part is constituted by the sum of the products of the Lagrange multipliers λ and the complicating constraints h coming from Zone b.

As indicated by the superscripts, the Lagrange multipliers come from Zone b of the last OCD iteration from the complicating constraints $h_{i,k}^{\text{hydr,sn,bi,zb}}$ and $h_{i,k}^{\text{therm,bi,zb}}$ of the respective border nodes. The complicating constraints itself are utilized in the slight modified form given below in (29)–(31) with the additional obj superscript. In comparison to (22), (24) and (26), all variables become OCD parameters and vice versa. Furthermore, all sets that were based on Zone a now become dependent on Zone b and the other way around. This leads to the following definitions:

$$h_{i,k}^{\text{obj,hydr,sn,bi,zb}} = \sum_{\substack{e\in\mathbb{S}_e \\ e\notin\mathbb{S}_e^{\text{be}}}} A_{i,e}\overline{\dot{m}}_{e,k}+\sum_{e\in\mathbb{S}_e^{\text{be}}} A_{i,e}\dot{m}_{e,k}=0 \qquad \forall\, i\in\mathbb{S}_i^{\text{sn,bi,z}}, k\in\mathbb{S}_k \tag{29}$$

where the border edge mass flow is defined similarly as in (24) by:

$$\dot{m}_{e,k}\approx\frac{1}{\sqrt{\mu_{e,k}^{\text{pre}}}}\frac{\sum_{i\in\mathbb{S}_i^{\text{bi,zb}}}\left(|A_{i,e}|\overline{p}_{i,k}-\sum_{i'\neq i\in\mathbb{S}_i}|A_{i',e}|p_{i',k}\right)}{\sqrt{\left|\sum_{i\in\mathbb{S}_i^{\text{bi,zb}}}\left(|A_{i,e}|\overline{p}_{i,k}-\sum_{i'\neq i\in\mathbb{S}_i}|A_{i',e}|p_{i',k}\right)\right|_{\Delta\varepsilon}}} \qquad \forall\, e\in\mathbb{S}_e^{\text{be,zb}}, k\in\mathbb{S}_k \tag{30}$$

The thermal node equation is formulated as follows for border nodes:

$$
\begin{aligned}
h_{i,k}^{\mathrm{obj,therm,bi,zb}} = \overline{T}_{i,k} \Bigg[& \sum_{\substack{e \in \mathbb{S}_e^{\mathrm{zb}} \\ e \notin \mathbb{S}_e^{\mathrm{zb,be}}}} \left(A_{i,e}^{-} \max\left(\overline{\dot{m}}_{e,k}, 0\right) + A_{i,e}^{+} \max\left(-\overline{\dot{m}}_{e,k}, 0\right) \right) + \\
& \sum_{e \in \mathbb{S}_e^{\mathrm{zb,be}}} \left(A_{i,e}^{-} \max\left(\dot{m}_{e,k}, 0\right) + A_{i,e}^{+} \max\left(-\dot{m}_{e,k}, 0\right) \right) \Bigg] \\
- \Bigg[& \sum_{\substack{e \in \mathbb{S}_e^{\mathrm{zb}} \\ e \notin \mathbb{S}_e^{\mathrm{zb,be}}}} \left(A_{i,e}^{+} \max\left(\overline{\dot{m}}_{e,k}, 0\right) \overline{T}_{e,k}^{\mathrm{out}} + A_{i,e}^{-} \max\left(-\overline{\dot{m}}_{e,k}, 0\right) \overline{T}_{e,k}^{\mathrm{in}} \right) + \\
& \sum_{e \in \mathbb{S}_e^{\mathrm{zb,be}}} \left(\left(A_{i,e}^{+} \max\left(\dot{m}_{e,k}, 0\right) + A_{i,e}^{-} \max\left(-\dot{m}_{e,k}, 0\right) \right) \sum_{\substack{i' \neq i \\ i' \in \mathbb{S}_i}} |A_{i,e}||A_{i',e}| T_{i',k} \right) \\
\Bigg] = 0 & \qquad \forall\, i \in \mathbb{S}_i^{\mathrm{bi,zb}}, k \in \mathbb{S}_k
\end{aligned}
\tag{31}
$$

Therein, the border mass flows are defined by (30).

The overall subproblem for Zone a then comprises the objective function (28), the complicating constraints (21) and (26) for the respective border nodes of Zone a, the equality constraints listed in Section 3.1.2 for all other network components in Zone a, as well as box constraints limiting the solution set.

4. Results

Two examples demonstrating the applicability range of the described method to the distributed optimal operation of DHNs are considered. The *eight-node network*, as depicted in Figure 2, extends the *four-node network* introduced in Section 3.2 and depicted in Figure 1, by modeling the thermal properties of the pipes dynamically. Each example network was solved in both a centralized and a distributed manner using OCD. We found that distributed and central optimization problems converged to identical solutions in both considered examples. However, the OCD convergence properties for the *eight-node network* is highly dependent on the used parameter set.

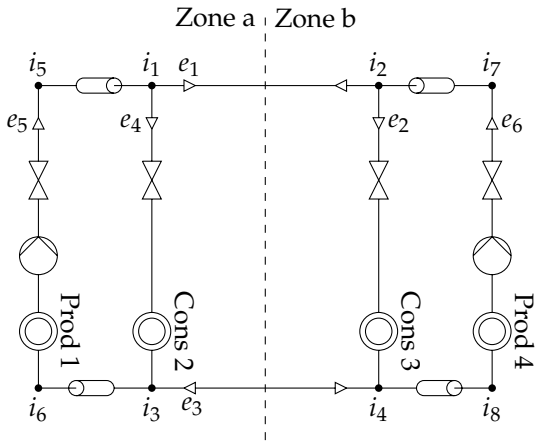

Figure 2. Example: *eight-node network*. DHN with eight nodes and dynamic elements decomposed into Zones a and b.

The central problem was solved using the *Interior Point Optimizer (IPOPT)* [34]. The steps of the OCD procedure were implemented as optimization problems with an iteration limit of one, calling IPOPT once per step and zone.

4.1. Parameterization

The the values and bounds of the variables used in the following examples are given in Table 1. The *Lagrangian modification parameter* δ ensures a non-singular Hessian of the Lagrangian by adding $\delta\mathbf{I}$ to the aforementioned.

Table 1. The parameters used for simulation. The values are equal for all time steps $k \in \mathbb{S}_k$.

(a) Constants			
Description	**Symbol**	**Value**	
Constant predefined pressure	p^{pre}	3 bar	
Lagrangian modification parameter	δ	1×10^{-11}	
Predefined quadratic component coefficient	$\mu^{\text{pre}}_{e_1,k}$	$100\,\text{bar}\,\text{s}^2\,\text{kg}^{-2}$	
Quadratic component coefficients	$\mu_{e_5,k}$ $\mu_{e_6,k}$	0	
Constant component coefficients	$\beta_{e_2,k}$ $\beta_{e_4,k}$	0	
Marginal bid prices	$c_{e_2,k}$ $c_{e_4,k}$ $c_{e_5,k}$ $c_{e_6,k}$	5 8 1 10	
(b) Bounded Variables			
Description	**Symbol**	**Minimum**	**Maximum**
Nodal pressures	$p_{i,k}$	0	p^{pre}
Mass flow rates	$\dot{m}_{e,k}$	0	$2\,\text{kg}\,\text{s}^{-1}$
Inlet temperatures Outlet temperatures	$T^{\text{in}}_{e,k}$ $T^{\text{out}}_{e,k}$	70 °C 70 °C	100 °C 100 °C
Nodal temperatures	$T_{i,k}$	70 °C	100 °C
Thermal power supply (producers)	$\Phi_{e_2,k}$ $\Phi_{e_4,k}$	0	40 kW
Thermal power demand (consumers)	$\Phi_{e_5,k}$ $\Phi_{e_6,k}$	−40 kW	0
Quadratic component coefficient	$\mu_{e,k}$	$0.9\,\text{bar}\,\text{s}^2\,\text{kg}^{-2}$	$1.1\,\text{bar}\,\text{s}^2\,\text{kg}^{-2}$

In addition to the parameters given in Table 1, the *eight-node network* considers identical pipes of diameter 100 mm with a surface roughness of 0.4 mm. The pipe length is set to 50 m.

All parameters are equal for all times steps k. Therefore, it is sufficient to consider a single time step in the *four-node network*; however, the dynamic elements in the *eight-node network* warrant the consideration of multiple time steps. The following considers six time steps of 5 min each.

4.2. Dimensionality Reduction

The *four-node network* problem optimizes a total of 28 variables, the *eight-node network* a total of 432. Thus, the results must be presented in aggregated form. This subsection introduces the methods used to do so.

4.2.1. Maximum Infeasibility

Given the optimization variables $\mathbf{x}$ and the the active constraints $\mathbf{h}(\mathbf{x}) = \mathbf{0}$, the *maximum infeasibility* at $\mathbf{x}$ is defined as the ℓ^∞-norm of $\mathbf{h}(\mathbf{x})$. Note, that for any $\mathbf{v} \in \mathbb{R}^N$, its ℓ^∞-norm is given by $\|\mathbf{v}\|_\infty = \max\{v_1, \ldots, v_N\}$. By definition a solution to any optimization problem must satisfy its constraints corresponding to a *maximum infeasibility* of zero. In practice, a value of zero is difficult to obtain numerically; thus, the following will be content

with small values. An initial point may, and in the following does, violate the constraints yielding a non-zero *maximum infeasibility*.

4.2.2. Representative Pressures

Note that (20) allows the definition of $p_{i_3,k}$ and $p_{i_4,k}$ in terms of $p_{i_1,k}$ and $p_{i_2,k}$ and the combination of (14) and (11) gives an injective relationship between the nodal pressures $p_{i,k}$ and the mass flow rates $\dot{m}_{e,k}$. Therefore, $p_{i_1,k}$ and $p_{i_2,k}$ are sufficient for the study of any feasible hydraulic state of either example network without loss of generality. As shown in Figure 3, intermediate states may be infeasible in some steps of the iteration process.

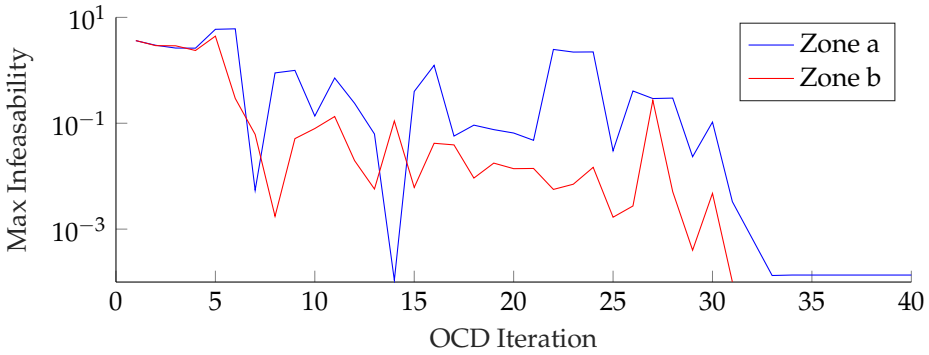

Figure 3. Maximum infeasibility per zone when solving the *four-node network* using flat initialization.

4.2.3. Mean Square Error

The *Mean Square Error* (MSE) was used as a metric for measuring the difference of a central and distributed solution unifying all relevant variables in a single metric according to the definition

$$\mathrm{MSE} = \frac{1}{n} \sum_{k \in \mathbb{S}_k} \sum_{e \in \mathbb{S}_e} \sum_{i \in \mathbb{S}_i} \left(\left(\frac{\Delta \dot{m}_{e,k}}{2\,\mathrm{kg\,s^{-1}}} \right)^2 + \left(\frac{\Delta p_{i,k}}{3\,\mathrm{bar}} \right)^2 + \left(\frac{\Delta T_{i,k}}{30\,\mathrm{K}} \right)^2 + \left(\frac{\Delta \Phi_{e,k}}{40\,\mathrm{kW}} \right)^2 \right) \tag{32}$$

where Δ denotes the difference of the central and distributed solutions in the corresponding variable. Any edges that are neither consumers nor producers do not define a thermal power $\Phi_{e,k}$ and are therefor ignored. Division by the number of variables summed in n, with $n = |\mathbb{S}_k| \left(|\mathbb{S}_e| + 2|\mathbb{S}_i| + \left|\mathbb{S}_e^{\mathrm{exch}}\right| \right)$, produces values on a similar order of magnitude independent of network size. The normalization constants correspond to the ranges set for the respective variables as defined in Table 1b, ensuring that individual variables will not typically dominate the value of the MSE and guaranteeing unit-less results. Note that this definition does neither assume nor require feasibility.

4.3. Initialization

The *four-node network* was solved with all optimization variables initially set to zero. This *flat* initialization ignores any constraints placed on the variables. Convergence to the central solution was reached after 28 iterations. If the hydraulic equations contained in the model are solved beforehand in a so called *hydraulic pre-calculation* the obtained starting point can reduce the number of iterations needed. In the *four-node network* example this reduces the number of iterations to 25. The *eight-node network* requires a hydraulic pre-calculation as it does not converge using flat initialization, which is known in the literature, see, e.g., [4] for similar observations.

4.4. Four Node Network with Flat Initialization

Figure 4a shows the nodal pressures $p_{1,1}$ and $p_{2,1}$ in the *four-node network*, and therefore it is in a hydraulic state. The dashed line indicates the central solution. As depicted, the distributed solution converges to the central solution in 32 iterations. IPOPT took 28 iterations to solve the central problem. Figure 4b shows the thermal powers of the

consumers and producers, demonstrating that convergence is not isolated to the hydraulic variables. Figure 4c aggregates all relevant variables according to (32).

As shown in Figure 3, the initial point is infeasible. Throughout the OCD steps, the *maximum infeasibility* tends to decrease.

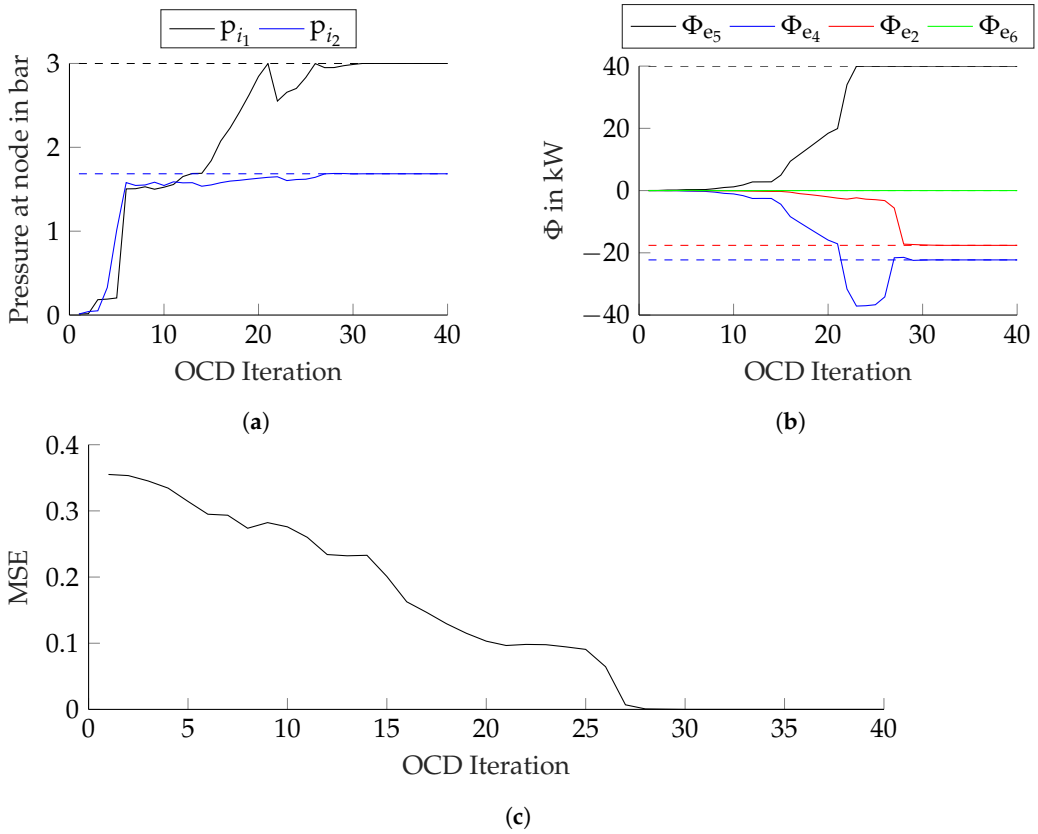

Figure 4. *Four-node network* from Figure 1 solved from an initial point with all variables set to zero. (**a**) Pressures at nodes one and two; (**b**) Thermal power output/consumption of consumers and producers; (**c**) Mean Square Error as defined in (32).

4.5. Eight Node Network with Hydraulic Pre-Calculation

Figure 5 shows that the *eight-node network* example converges in 126 iterations. IPOPT required 69 iterations to solve the central problem.

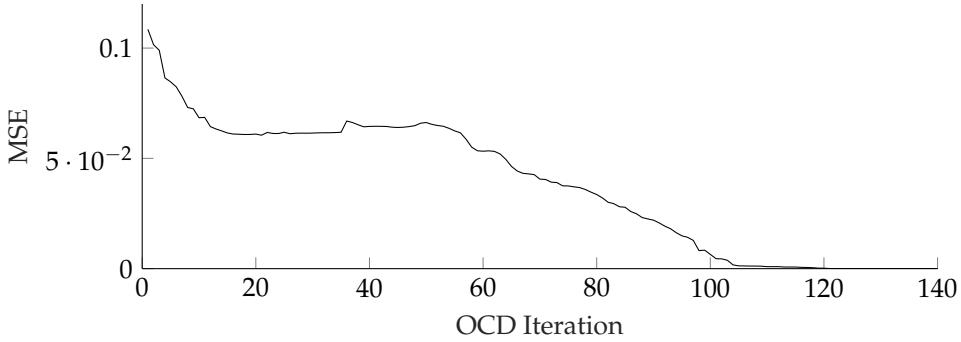

Figure 5. MSE while solving the *eight-node network* from Figure 2 using initialization based on hydraulic pre-calculation.

4.6. Computation Time

An *Intel i7-10700T* CPU was used at a clock speed of 4.5 GHz to test the run time of the given examples. Table 2 summarizes the obtained results. The time given is the total

time spend evaluating objective functions, constraints, their derivatives and completing optimization steps in *IPOPT* but excluding any boilerplate code for setting up, progress monitoring and switching zones.

In the OCD approach the zones where optimized sequentially to avoid zones influencing each others performance by accessing the same cash but the time given in Table 2 assumes parallel execution. The computation time depends on the specifics of the machine used for testing, however the ratio of the run times for the OCD and central approaches as given in Table 2 stays ruffly constant across differing hardware and is therefore more meaningful than absolute computation times. Knowledge of the central solution was used to terminate the OCD iteration as soon as the MSE fell below 3×10^{-10}.

Table 2. Computation time and iteration counts for the considered examples.

Example	Central/OCD	Iterations	Time in ms	$\frac{\text{OCD Time}}{\text{Central Time}}$
Four Node Network	Central OCD	28 32	13 117	9.0
Eight Node Network	Central OCD	69 126	495 1248	2.5

As shown in Table 2 the OCD solution is significantly slower as the central solution. However the advantage of the central solution is smaller for the larger example considered. This matches the results obtained in [22], where OCD becomes much faster as the central solution for larger networks. Hence, this leads to the assumption that OCD will be faster for a sufficiently large network.

4.7. Other Solutions

With other parameter sets, the decomposed problem was observed to converge to other solutions. For example, increasing the marginal bid price of the consumer on e_4 from 5 to 6 produces the results shown in Figure 6 and caused the OCD approach to converge to a solution distinct from that of the central approach. The MSE was found to plateau after 100 iterations at a value of 0.08. The final objective value of the distributed solution was 0.35 % better than in the central case; however, while the central solution solves all constraints to an infeasibility of at least 1×10^{-13} the distributed solution shows maximum infeasibilites in the order of 1×10^{-4}.

The results of further increasing the marginal bid price of the consumer e_4 to 12 are shown in Figure 7 and causes the OCD approach to fail as no convergence is observed with even the best set of values reached through out the OCD procedure violating the constraints by an infeasibility of at least 1×10^{-2}. After iteration 130 the MSE oscillated around a value of 0.075 corresponding to a 4.9 % better objective value compared to the central case.

While the OCD approach converged to the central solution for the prevailing amount of parameters tested in the *four-node network*, the distributed solution of the *eight-node network* only converged toward the central solution in a minority of the considered parameter sets. A potential explanation for this result is that the *eight-node network* case, which in contrast to the *four-node network* includes the thermal pipeline models, Condition 1 might be violated regularly.

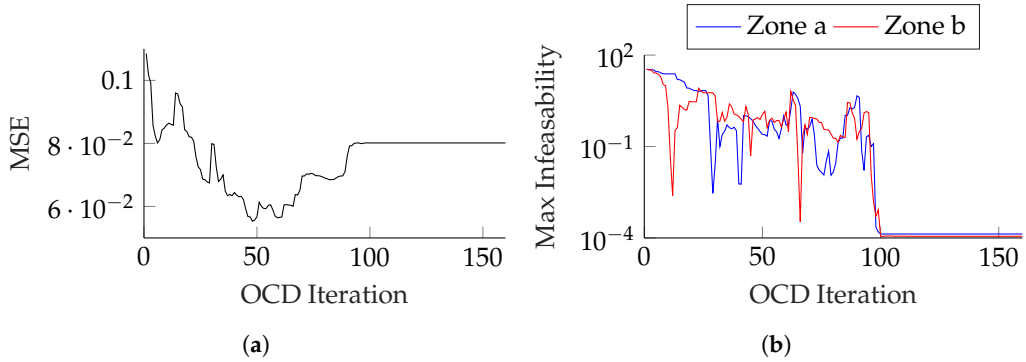

(**a**) (**b**)

Figure 6. *Eight-node network* with the marginal bid price c_{e_4} increased to 6. Initialization based on Hydraulic Pre-Calculation. (**a**) MSE as defined in (32); (**b**) Maximum infeasability per zone.

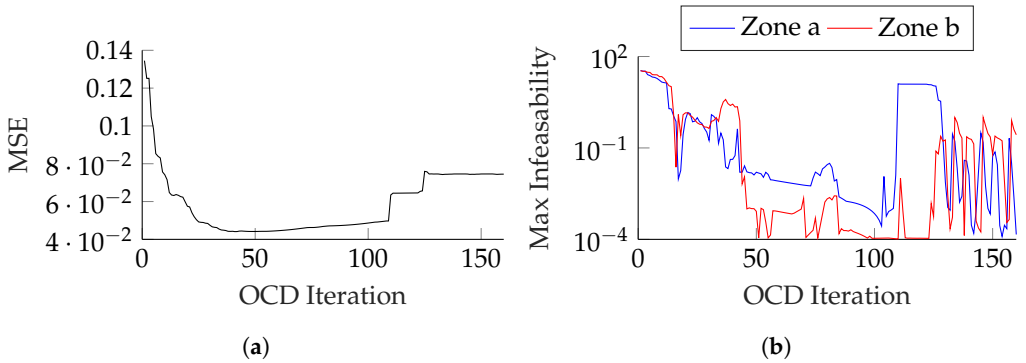

(**a**) (**b**)

Figure 7. *Eight-node network* with the marginal bid price c_{e_4} increased to 12. Initialization based on Hydraulic Pre-Calculation. (**a**) MSE as defined in (32). (**b**) Maximum infeasability per zone.

5. Discussion

The presented approach shows how OCD can be applied to the optimal operation of DHNs. As explained, several difficulties need to be overcome to enable the application of OCD to DHNs. This includes the strong coupling of the subproblems resulting from the symmetric flow conditions in supply and return networks in DHNs. While the concept shows good convergence properties for the *four-node network* for the majority of the tested parameter sets, the results indicate that further work is needed to enhance the convergence of the distributed solution towards the central solution for the regarded dynamic *eight-node network* and thus likely also for networks with even more components. Hence, the presented ideas to circumvent the strong coupling of the subproblems appearing from the application of the OCD method to DHNs may need to be further extended for large-scale DHNs.

Author Contributions: Conceptualization, J.M. and S.H.; methodology, J.M.; software, J.M. and J.I.; validation, J.M., J.I. and P.J.S.; formal analysis, J.M., J.I., P.J.S. and S.H.; investigation, J.M. and J.I.; resources, S.H.; writing—original draft preparation, J.M.; writing—review and editing, J.I., P.J.S. and S.H.; visualization, J.M. and J.I.; supervision, S.H.; project administration, S.H.; funding acquisition, S.H. All authors have read and agreed to the published version of the manuscript.

Funding: This research is funded by the Helmholtz Association and by Germany's Federal Ministry for Economic Affairs and Energy within the project RegEnZell (0350062A). We acknowledge support by the KIT-Publication Fund of the Karlsruhe Institute of Technology.

Data Availability Statement: Data is contained within the article.

Conflicts of Interest: The authors declare no conflict of interest.

Abbreviations

The following abbreviations are used in this manuscript:

ADMM	Alternating Direction Method of Multipliers
DHN	District Heating Network
EMS	Energy Management System
KKT	Karush–Kuhn–Tucker
MSE	Mean Square Error
NLP	Nonlinear Programming
OCD	Optimality Condition Decomposition
VMFD	Variable Mass Flow Direction

Nomenclature

Symbols

$\boldsymbol{A}$	Node edge incidence matrix
$\boldsymbol{A}^-$	Node leaving edge incidence matrix
$\boldsymbol{A}^+$	Node incoming edge incidence matrix
β	Constant component coefficient
B^{bus}	Susceptance of nodal admittance matrix element
c	Bid/Offer price per unit
c^{w}	Specific heat capacity of water
δ	Lagrangian modification parameter
$\Delta\varepsilon$	Small positive parameter
Δh	Height difference
$\boldsymbol{\Delta\lambda}^{\text{cent}}$	Vector of change of dual variables within two iterations for the central case
$\boldsymbol{\Delta\lambda}^{\text{dist}}$	Vector of change of dual variables within two iterations for the distributed case
Δp	Pressure Difference
$\boldsymbol{\Delta x}^{\text{cent}}$	Vector of change of optimization variables within two iterations for the central case
$\boldsymbol{\Delta x}^{\text{dist}}$	Vector of change of optimization variables within two iterations for the distributed case
f	Objectiv function
f^{rest}	Part of objective function not resulting from OCD approach
G^{bus}	Conductance of nodal admittance matrix element
h	Equality constraints
$\boldsymbol{h}$	Vector of equality constraints
$\boldsymbol{I}$	Identity matrix
$\mathbf{KKT}$	Karush-Kuhn-Tucker (KKT) matrix
$\overline{\mathbf{KKT}}$	Approximated Karush-Kuhn-Tucker (KKT) matrix
$\boldsymbol{\lambda}$	Vector of dual variables
$\dot{m}$	Mass flow
μ	Quadratic component coefficient
n	Number of variables in MSE
$\nabla \boldsymbol{h}$	Jacobian matrix of the equality constraints
$\nabla \boldsymbol{\mathcal{L}}$	Jacobian matrix of the Lagrangian
P^{flow}	Real power flow between two buses
Φ	Heat power
p	Pressure potential
$\rho^{\text{ocd},*}$	Least linear congervence rate of Optimality Condition Decomposition (OCD) approach
R, S, y, z	Precalculated values in thermal pipeline model
$\mathbb{S}$	Set
T	Temperature
θ	Voltage angle
T^{in}	Input temperature
T^{out}	Outlet temperature

V	Voltage amplitude
$\boldsymbol{x}$	Variable vector
$\boldsymbol{y}^0$	Starting point for optimization
$\boldsymbol{y}^*$	Second-order Karush-Kuhn-Tucker (KKT) point
Indices	
0	Initial state
e	Edge
i	Node
k	Time step
l	Loop
ν	Iteration of distributed optimization approach
+	Incoming edge, positive flow direction
−	Leaving edge, negative flow direction
be	Border edge
bi	Border node
bl	Border loop
cent	Central
dist	Distributed
exch	Heat exchanger
flow	(Line) Flow
hydr	Hydraulic
in	Input of edge
max	Maximum
min	Minimum
obj	Objective
ocd	Optimality Condition Decomposition (OCD)
out	Outlet of edge
pre	Predefined before optimization
rn	Return network
sn	Supply network
$*$	(At) Optimal point
vmfd	Variable Mass Flow Direction (VMFD)
w	Water
za	Zone a
zb	Zone b

References

1. Moustakidis, S.; Meintanis, I.; Halikias, G.; Karcanias, N. An innovative control framework for district heating systems: conceptualisation and preliminary results. *Resources* **2019**, *8*, 27. [CrossRef]
2. Sameti, M.; Haghighat, F. Optimization approaches in district heating and cooling thermal network. *Energy Build.* **2017**, *140*, 121–130. [CrossRef]
3. Zheng, J.; Zhou, Z.; Zhao, J.; Wang, J. Effects of the operation regulation modes of district heating system on an integrated heat and power dispatch system for wind power integration. *Appl. Energy* **2018**, *230*, 1126–1139. [CrossRef]
4. Tröster, S. *Zur Betriebsoptimierung in Kraft-Wärme-Kopplungssystemen unter Berücksichtigung der Speicherfähigkeit des Fernwärmenetzes*; Fraunhofer-IRB-Verlag: Oberhausen, Germany, 1999.
5. Zheng, J.; Zhou, Z.; Zhao, J.; Wang, J. Integrated heat and power dispatch truly utilizing thermal inertia of district heating network for wind power integration. *Appl. Energy* **2018**, *211*, 865–874. [CrossRef]
6. Zhang, M.; Wu, Q.; Wen, J.; Lin, Z.; Fang, F.; Chen, Q. Optimal operation of integrated electricity and heat system: A review of modeling and solution methods. *Renew. Sustain. Energy Rev.* **2021**, *135*, 110098. [CrossRef]
7. Sauter, P.S. Modellierung und Zentrale Prädiktive Regelung von Multimodalen Energieverteilnetzen. Ph.D. Thesis, Karlsruher Institut für Technologie (KIT), Karlsruhe, Germany, 2019. [CrossRef]
8. Li, H.; Svendsen, S.; Gudmundsson, O.; Kuosa, M.; Rämä, M.; Sipilä, K.; Blesl, M.; Broydo, M.; Stehle, M.; Pesch, R.; et al. *Future Low Temperature District Heating Design Guidebook: Final Report of IEA DHC Annex TS1. Low Temperature District Heating for Future Energy Systems*; Technical Report; AGFW-Project Company: Frankfurt am Main, Germany, 2017.
9. Molzahn, D.K.; Dörfler, F.; Sandberg, H.; Low, S.H.; Chakrabarti, S.; Baldick, R.; Lavaei, J. A survey of distributed optimization and control algorithms for electric power systems. *IEEE Trans. Smart Grid* **2017**, *8*, 2941–2962. [CrossRef]
10. Conejo, A.J.; Castillo, E.; Minguez, R.; Garcia-Bertrand, R. *Decomposition Techniques in Mathematical Programming: Engineering and Science Applications*; Springer Science & Business Media: Berlin/Heidelberg, Germany, 2006. [CrossRef]

11. Liang, X.; Li, Z.; Huang, W.; Wu, Q.; Zhang, H. Relaxed Alternating Direction Method of Multipliers for Hedging Communication Packet Loss in Integrated Electrical and Heating System. *J. Mod. Power Syst. Clean Energy* **2020**, *8*, 874–883. [CrossRef]
12. Lin, C.; Wu, W.; Zhang, B.; Sun, Y. Decentralized solution for combined heat and power dispatch through benders decomposition. *IEEE Trans. Sustain. Energy* **2017**, *8*, 1361–1372. [CrossRef]
13. Lu, S.; Gu, W.; Zhou, S.; Yu, W.; Yao, S.; Pan, G. High-resolution modeling and decentralized dispatch of heat and electricity integrated energy system. *IEEE Trans. Sustain. Energy* **2019**, *11*, 1451–1463. [CrossRef]
14. Tan, J.; Wu, Q.; Wei, W.; Liu, F.; Li, C.; Zhou, B. Decentralized robust energy and reserve Co-optimization for multiple integrated electricity and heating systems. *Energy* **2020**, *205*, 118040. [CrossRef]
15. Xu, D.; Wu, Q.; Zhou, B.; Li, C.; Bai, L.; Huang, S. Distributed multi-energy operation of coupled electricity, heating, and natural gas networks. *IEEE Trans. Sustain. Energy* **2019**, *11*, 2457–2469. [CrossRef]
16. Arnold, M.J. On Predictive Control for Coordination in Multi-Carrier Energy Systems. Ph.D. Thesis, ETH Zurich, Zurich, Switzerland, 2011.
17. Huang, J.; Li, Z.; Wu, Q. Coordinated dispatch of electric power and district heating networks: A decentralized solution using optimality condition decomposition. *Appl. Energy* **2017**, *206*, 1508–1522. [CrossRef]
18. Xue, Y.; Li, Z.; Lin, C.; Guo, Q.; Sun, H. Coordinated dispatch of integrated electric and district heating systems using heterogeneous decomposition. *IEEE Trans. Sustain. Energy* **2019**, *11*, 1495–1507. [CrossRef]
19. Wang, X.; Bie, Z.; Liu, F.; Kou, Y. Co-optimization planning of integrated electricity and district heating systems based on improved quadratic convex relaxation. *Appl. Energy* **2021**, *285*, 116439. [CrossRef]
20. Boyd, S.; Parikh, N.; Chu, E.; Peleato, B.; Eckstein, J. Distributed optimization and statistical learning via the alternating direction method of multipliers. *Found. Trends Mach. Learn.* **2011**, *3*, 1–122. [CrossRef]
21. Conejo, A.J.; Nogales, F.J.; Prieto, F.J. A decomposition procedure based on approximate Newton directions. *Math. Program.* **2002**, *93*, 495–515. [CrossRef]
22. Guo, J.; Hug, G.; Tonguz, O.K. Intelligent partitioning in distributed optimization of electric power systems. *IEEE Trans. Smart Grid* **2016**, *7*, 1249–1258. [CrossRef]
23. Kaisermayer, V.; Muschick, D.; Horn, M.; Gölles, M. Operation of coupled multi-owner district heating networks via distributed optimization. *Energy Rep.* **2021**, *7*, 273–281. [CrossRef]
24. Nogales, F.J.; Prieto, F.J.; Conejo, A.J. A decomposition methodology applied to the multi-area optimal power flow problem. *Ann. Oper. Res.* **2003**, *120*, 99–116. [CrossRef]
25. Arnold, M.; Knopfli, S.; Andersson, G. Improvement of OPF decomposition methods applied to multi-area power systems. In Proceedings of the 2007 IEEE Lausanne Power Tech, Lausanne, Switzerland, 1–5 July 2007; pp. 1308–1313. [CrossRef]
26. Maurer, J.; Golla, A.; Richter, B.; Hohmann, S.; Weinhardt, C. Hybrid Pricing Based Operation of Coupled Electric Power and District Heating Networks. *Sustain. Energy Grids Netw.* **2021**, *28*, 100532. [CrossRef]
27. Oppelt, T.; Urbaneck, T.; Gross, U.; Platzer, B. Dynamic thermo-hydraulic model of district cooling networks. *Appl. Therm. Eng.* **2016**, *102*, 336–345. [CrossRef]
28. Brkić, D. Review of explicit approximations to the Colebrook relation for flow friction. *J. Pet. Sci. Eng.* **2011**, *77*, 34–48. [CrossRef]
29. Li, Z.; Wu, W.; Shahidehpour, M.; Wang, J.; Zhang, B. Combined Heat and Power Dispatch Considering Pipeline Energy Storage of District Heating Network. *IEEE Trans. Sustain. Energy* **2015**, *7*, 12–22. [CrossRef]
30. Liu, X.; Wu, J.; Jenkins, N.; Bagdanavicius, A. Combined analysis of electricity and heat networks. *Appl. Energy* **2016**, *162*, 1238–1250. [CrossRef]
31. Benonysson, A. Dynamic Modelling and Operational Optimization of District Heating Systems. Ph.D. Thesis, Technical University of Denmark, Lyngby, Denmark, 1991.
32. Maurer, J.; Ratzel, O.; Malan, A.J.; Hohmann, S. Comparison of Discrete Dynamic Pipeline Models for Operational Optimization of District Heating Networks. *Energy Rep.* **2021**, *7*, 244–253. [CrossRef]
33. Nocedal, J.; Wright, S.J. *Numerical Optimization*, second ed.; Springer Series in Operation Research and Financial Engineering; Springer: New York, NY, USA, 2006. [CrossRef]
34. Wächter, A.; Biegler, L.T. On the implementation of an interior-point filter line-search algorithm for large-scale nonlinear programming. *Math. Program.* **2006**, *106*, 25–57. [CrossRef]